Bull Volcanol (2003) 65:90–104
DOI 10.1007/s00445-002-0244-z

RESEARCH ARTICLE

Oliver Spieler · Mikhail Alidibirov · Donald B. Dingwell

Grain-size characteristics of experimental pyroclasts of 1980 Mount St. Helens cryptodome dacite: effects of pressure drop and temperature

Received: 24 April 2001 / Accepted: 15 August 2002 / Published online: 7 November 2002

Abstract Using the fragmentation bomb, we analysed the effects of temperature and pressure drop on the grain-size characteristics of experimentally produced pyroclasts. Experiments performed on vesicular samples of grey dacite of the 1980 Mount St. Helens cryptodome at T=20–900 °C and initial pressure differential up to 18.5 MPa provide clear evidence of the influence of these physical conditions upon fragment size and character. Cylindrical dacite samples (diameter=17 mm, length=50 mm) are placed in the high-pressure-temperature section of the apparatus, heated and saturated by argon gas. The disruption of a diaphragm located between the high- and low-pressure sections of the apparatus initiates the rapid depressurisation of the sample. The main results may be summarised as follows. (1) Increasing temperature from 20 to 900 °C results in a decrease in the fragmentation threshold value from 9 to 3 MPa, and an increase in the median diameter of the experimental pyroclasts. These observations imply a decrease in the dynamic tensile strength of dacite at higher temperatures which in turn influences the characteristic size of fragments. (2) Increasing initial pressure differential yields a decrease of the median diameter. Thus, a higher initial elastic potential energy in the magma generates a higher degree of fragmentation. (3) Fragments of angular shape are observed from experiments at all investigated temperatures (20–900 °C), including thereby temperatures significantly higher than the classical (dilatometrically or calorimetrically determined) glass transition temperature determined for this dacite of 810 °C. Thus, brittle response of the dacite is observed under rapid decompression. (4) Fragment size distributions do not correspond to log-normal distributions and are more closely described by Rosin-Rammler distributions. With a decrease of temperature and increase of the initial pressure differential, fragment size distributions approach a Rosin-Rammler distribution dependence. (5) Microscopic and grain-size comparison of particle characteristics of experimental and natural fragments of the 1980 Mount St. Helens cryptodome dacite demonstrate similar median diameters and shapes.

Keywords Fragmentation · Pyroclast · Mount St. Helens · Dacite · Grain-size distribution · Experimental · Volcanology

Editorial responsibility: M. Carroll

O. Spieler (✉) · M. Alidibirov · D.B. Dingwell
Earth and Environmental Science, University of Munich,
Theresienstrasse 41, 80333 Munich, Germany
e-mail: spieler@impg-muenchen.de
Tel.: +49-89-2180-4221
Fax: +49-89-2180-4176

Introduction

Inevitably, in the course of explosive volcanic eruptions, fragmentation of magma occurs. In fact, the production of pyroclasts and especially volcanic ash by fragmentation is the defining feature of explosive eruptions. Despite this clear link, our understanding of the nature of magma fragmentation is far from complete. For this reason, the processes controlling the explosive degassing of magma have been the subject of vigorous debate for the past three decades (McBirney and Murase 1970; Bennet 1974; Sparks 1978; Wohletz et al. 1984; Dingwell and Webb 1989, 1990; Webb and Dingwell 1990; Heiken and Wohletz 1991; Fink and Kieffer 1993; Proussevich et al. 1993; Alidibirov 1994; Cashman and Mangan 1994; Hurwitz and Navon 1994; Sparks et al. 1994; Thomas et al. 1994; Barclay et al. 1995; Dingwell 1996; Sparks 1997; Neri et al. 1998; Papale et al. 1998; Papale 1998, 1999; Melnik and Sparks 1999; Sahagian 1999; Zhang 1999; Melnik 2000; Voight and Elsworth 2000; Alidibirov and Dingwell 2000; Spieler 2001; Ichihara et al. 2001).

A fundamental challenge to the investigation of particle-size distribution data of natural pyroclasts lies in inferring the initial distribution in the eruption cloud near the vent immediately after fragmentation. This is because studies of explosive eruptions must rely on grain-size characteristics of pyroclastic deposits containing materials which have been processed by transport from

the vent by one or a combination of processes (Kittleman 1964; Wohletz et al. 1989; Wohletz and Brown 1995). Despite attempts to calculate the pristine particle size distribution in the eruption column (e.g. Koyaguchi 1994), this problem is not yet fully resolved. One problem, which is currently debated as a result, is whether or not the pristine particle size distribution of pyroclasts corresponds to a log-normal or a Rosin-Rammler distribution (Dellino and La Volpe 1995). Further influence concerning the pristine particle distribution and the change of the distribution due to transport processes are discussed by Wohletz et al. (1989) and Brown and Wohletz (1995). A second problem concerns the determination of the mechanism of magma fragmentation which, together with estimation of the influence of physical variables on the fragmentation process (pressure, temperature, decompression rate) and the character of the resulting pyroclasts, should allow interpolation/extrapolation to natural situations. In order to address such questions, experimental approaches to magma fragmentation are clearly needed.

During the past decade, a number of laboratory simulations of magma fragmentation using analogue liquids and shock-tube type apparatus have been developed. As process triggers, they have employed explosive vaporisation of superheated liquids (Hill and Sturtevant 1990; Sugioka and Bursik 1995); rapid mixing of concentrated K_2CO_3 and HCl and decompression of CO_2-saturated water (Mader et al. 1994, 1996; Sparks et al. 1994) and CO_2–H_2O–polymer systems (Zhang et al. 1997); and rapid decompression of the gum rosin-acetone (GRA) system (Phillips et al. 1995). Very recently, these experiments have been augmented by rapid decompression experiments performed on viscoelastic analogue material (Ichihara et al., unpublished data). These experiments have revealed a wide variety of aspects of dynamics of vesiculation and fragmentation processes *but in none of the above have grain-size characteristics of the experimentally generated fragments been obtainable*. Thus, one potentially important source of experimental data constraining the nature of the fragmentation process is missing.

A clear advantage of experiments on natural magma samples is the opportunity to investigate the texture and grain-size characteristics of the produced fragments. Kaminski and Jaupart (1998) performed laboratory experiments on primary fragmentation (single event generated, i.e. piston fall experiments) and secondary fragmentation (multiple event generated, i.e. continuous milling experiments) in order to analyse the grain-size distribution of natural deposits. Their experiments on the primary fragmentation include external force by a piston and internal forced foam collapse as well as data from rapid decompression. Following Hartmann (1969) and Turcotte (1986), they discussed the primary fragment population ejected from the eruptive vent in the context of a power law distribution. The experimental approach using a piston for the study of the primary fragmentation appears to relate less to primary magma disruption in a vent than to the secondary fragmentation. Internal forces initialising a fragmentation, such as the rapid decompression experiments (Alidibirov and Dingwell 1996a, 1996b, 2000) act in a very different way. Here, we record a fragmentation layer travelling into the sample producing a time sequence of primary fragmentations. The high-temperature shock-tube type apparatus permits fragmentation of natural samples and is capable of delivering experimentally fragmented particles for grain-size analysis. This technique yielded the first experimental results for fragmentation of highly viscous samples of grey dacite of the 18 May 1980 Mount St. Helens eruption, at temperatures up to 915 °C (Alidibirov and Dingwell 1996a, 1996b). These experiments are likely to find their greatest relevance in application to the processes occurring during collapse events of lava domes and cryptodomes (Rose et al. 1977; Hoblitt et al. 1981; Voight 1981; Sato et al. 1992; Fink and Kiefer 1993; Voight and Elsworth 2000). The systematic dependence of the grain-size distribution statistics on experimental variables (temperature, pressure and decompression rate) is accessible since all the fragments generated can be collected and analysed. Further investigation of the influences of vesicle and crystal content on the fragmentation threshold and efficiency was performed on synthetic silicate melts by Martel et al. (2000, 2001). Experiments on the fragmentation of basaltic melts by injection of compressed air, and experiments on the interaction of water and silicate melts have also generated experimental pyroclasts (Zimanowski et al. 1986, 1991, 1995; Wohletz et al. 1995; Zimanowski et al. 1997a, 1997b). The pyroclasts presented below differ from those of hydromagmatic explosions in the post-fragmentation healing of surfaces of the later.

The main objectives of the present experiments on dacite fragmentation were (1) to determine the critical pressure drop causing dacite fragmentation at low and high temperatures (fragmentation threshold), (2) to determine the dependence of the median diameter and sorting coefficient of fragments on experimental temperature and pressure drop (differential), and (3) to compare grain-size distributions of fragments with empirical distribution functions (log-normal and Rosin-Rammler).

Methods

Experimental apparatus

The experimental apparatus has been described in detail by Alidibirov and Dingwell (1996b). It consists of a high-pressure-temperature (HPT) section and a low-pressure (LPT) section separated by a copper diaphragm scored with a pattern to ensure regular, reproducible rupture behaviour. The HPT section consists of a 450-mm-long tube with an external diameter of 40 mm and an internal diameter of 20 mm, which vents into a tank having a volume of ~0.7 m^3 (much larger than the volume of the high-pressure section which is ~8×10^{-5} m^3). This provides

an approximately constant pressure in the tank during the experiment. An external high-temperature foldaway furnace can be used to heat the HPT section.

During the low-temperature experiments; a sample is located inside a brass tube (internal diameter =17 mm; external diameter =20 mm) and is attached to the internal surface of this tube with glue (Crystalbond 509, Aremco, USA) to prevent gas from residing between the sample surface and the tube as well as to provide good adhesion of the sample to the tube walls. The tube with the sample is rigidly connected to the high-pressure section via a threaded closure. During the high-temperature experiments; the same geometry is used; but the sample holder is manufactured from Ni and a high-temperature cement (WH-Feuerfestkitt 1500, W. Haldenwanger, Berlin) is used to fix the sample into the tube.

Experimental materials

Cylindrical samples (length =50 mm, diameter =17 mm) of the 1980 Mount St. Helens cryptodome grey dacite were used in the present experiments. Light grey, vesicular, hypersthene-hornblende dacite was the most abundant juvenile lithology (72 vol%) erupted during the lateral blast of 18 May 1980 (Hoblitt et al. 1981; Eichelberger and Hayes 1982; Cashman 1988; Hoblitt and Harman 1993). The material used has a bulk density of 1.5×10^3 kg m^{-3}. The grey dacite contains ~30 vol% phenocrysts (on vesicle-free basis) of 210-μm average size, comprising plagioclase, hypersthene and hornblende and Fe–Ti oxides which are easily visible in SEM images of samples (Eichelberger and Hayes 1982; Cashman 1988).

It is important to note that pre-fragmented crystals exist in the cryptodome starting materials we have employed. These phenocrysts are shattered to smaller pieces whose sizes describe a log-normal distribution. The process of fragmentation was directed with the fractures yielding clear preferential orientations at 30–45° to the long axis of aligned crystals. In most cases these fractures are open and crystal particles are separated. We can only speculate about the energy source for this crystal fragmentation, since a highly energetic shock wave is likely to be necessary to produce such a feature in magma. Overpressure in melt inclusions may lower the needed energy and explain the open, gas-filled, inter-fracture spaces.

The proportion of microlites and microphenocrysts, typically plagioclase with widths of 1–10 μm, occupying some of the inter-bubble partitions of the groundmass is ~45 vol%, calculated on a vesicle-free basis from the BSE image of grey blast dacite in Cashman (1988). The material used has a total porosity of ~41.7 vol%. The closed porosity has been determined by measuring the true density of a crushed sample (powder <10 μm, 2.59×10^3 kg m^{-3}) obtained via helium pycnometry (AccuPyc 1330, Micromeritics, USA), and we calculated it against the pycnometricaly measured density of sample cylinders (2.34×10^3 kg m^{-3}) to be ~6.4 vol%. The open porosity was determined via density to be 35.3%, and consequently about 85% of all pores are interconnected. We have to take into account that all measurements were performed on cylindrical samples of 17- and 26-mm diameter – short range connections of <10–20 mm would be recognised as open porosity. Hg porosimetry performed on the dacite is discussed below. The majority of vesicles range in size between several microns width (average 5 μm) and several tens of microns, and are interconnected with a characteristic thickness of inter-bubble partitions of 1–4 μm (measured under the SEM). The glass transition temperature, dilatometrically measured, at a heating rate of 10 °C min^{-1} is T_g=800–810 °C. Above this temperature the bulk dacite is in a highly viscous state at time scales of a few seconds (e.g. at T=900 °C the viscosity of the dacite is $10^{10.8}$ Pa s; Alidibirov et al. 1997).

Experimental procedure

The experimental procedure consists of loading the sample in the high-pressure-temperature section, heating the HPT at a rate of ~10 °C min^{-1}, stabilising the temperature distribution over time, and slowly saturating the sample with argon, used as working gas, up to the pressure corresponding to the bursting pressure of the diaphragm. The argon is applied slowly to the HPT through an orifice 5 mm below the rupture disc. It fills the free space between the sample and the diaphragm (distance in all experiments=212 mm) as well as the open pores of the sample. In the experiments conducted at temperatures ≤810 °C (glass transition temperature), the argon supply is provided after heating the sample up to the desired temperature. For higher temperature experiments the gas is supplied in two stages. Firstly, after reaching the temperatures 750–800 °C, the gas pressure in the HPT section is raised to 80% of the diaphragm rupture pressure. Secondly, ~5 min after reaching the maximal experimental dwell temperature, samples are additionally pressurised up to the calibrated rupture pressure of the diaphragm. This procedure was undertaken to prevent possible shrinkage of the samples which occurs at T≥900 °C for this dacite (Alidibirov et al. 1997), and which would change the density and thus physical behaviour of the sample. The diaphragms (copper or steel) are scored with a design to precisely open at an experimentally calibrated, reproducible pressure. Accordingly, diaphragm rupture occurs at a certain pressure differential between the high-pressure and low-pressure section, causing the propagation of a shock wave in the direction of the LPT and the formation of a rarefaction wave which travels through the gas above the sample at the speed of sound (measured to be ~350 m s^{-1} at 10 MPa) into the high-pressure section. The rarefaction wave causes rapid decompression of the sample, and the resultant pressure history on the surface of the sample is a function of the initial pressure in the HPT and LPT, the

equation of state of the working gas, and the geometry (relative size) of the sections. The samples are rapidly depressurised and, if the pressure differential is high enough, the sample fragmentation occurs.

Two types of studies, aimed at understanding the influence of (1) temperature and (2) initial pressure differential on grain-size characteristics of fragments, have been performed.

1. The effect of temperature was investigated in a series of experiments in which the initial pressure differential was approximately constant at 12±0.4 MPa and initial temperature was varied. Four sets of experiments, each consisting of five to seven runs, were performed at selected temperatures (15–20, 750, 810 and 900 °C). Note that for the high-temperature experiments the temperatures are measured at the lower ends of the samples whereas the maximum temperature (at the centre of the 5-cm sample) is 15 °C higher. Thus, for experiments which are conducted at T=900 °C, for example, the maximum temperature in the centre of the sample was 915 °C.
2. The effect of pressure drop was investigated in two sets of experiments where the initial temperature were constant (T=20 and 900 °C respectively) and the initial argon gas pressure was varied within the range ΔP_0=1.0–18.5 MPa. The pressure inside the LPT was 0.1 MPa in all experiments.

Granulometry

After each experiment the fragments were sampled from the LPT for sieve analysis. The grain-size characteristics of the experimental fragments were obtained by processing the sieving data using the Inmann approach (Fisher and Schmincke 1984). Accordingly, φ units (φ=–$\log_2 d$ where d= diameter in mm) were used as a fragment size, and median diameter ($Md_\varphi=\varphi_{50}$), mean diameter ($M_\varphi=(\varphi_{16}+\varphi_{84})/2$) and sorting coefficient ($\sigma_\varphi=(\varphi_{84}-\varphi_{16})/2$), determined from cumulative curves, were used for characterisation of fragment grain-size distribution. Since the experimentally obtained grain-size distributions show almost single modality, we fulfilled the tight limitation of this approach. Multimodal distributions need a higher effort in the analysis using the sequential fragmentation/transport (SFT) model introduced by Wohletz et al. (1989). Particle size distributions of fragments were recalculated for their fit to log-normal and Rosin-Rammler laws using the program of Schleyer (1987).

The empirical Rosin-Rammler law describes the mass of fragments m_+ with size L, more than the mass of fragments m_0 with size L_0 as:

$$m_+/m_0 = \exp[-(L/L_0)^n] \quad (1)$$

This technique requires that the mass of the fragments is constant. In the typical petrological multiphase system, this assumption fails due to the mineral phases. Only in the case where the modal analysis proves that the phases are identically distributed in all grain sizes can we use this calculation.

$$-\ln\ln(m_+/m_0) = n(\ln L - \ln L_0). \quad (2)$$

From the expression above it is easy to compare the particle size distribution of experimental fragments to the Rosin-Rammler law. Note here that the Rosin-Rammler law corresponds to the Weibull distribution (Rodionov et al. 1986; Brown and Wohletz 1995). If the analysed fragments correspond to the ideal Rosin-Rammler distribution (Eq. 1), then they describe a linear array in the coordinate space, –ln ln(m_+/m_0), ln L, and from such plot parameters n and L can be determined where higher n means lower dispersion D–, such that fragments with size L are located closer to size L_0.

The log-normal distribution is described by the probability integral which can be expressed as:

$$\Phi(y) = \frac{1}{\sqrt{2\pi}} \int_{-\infty}^{y} e^{-\frac{y^2}{2}} dy \quad (3)$$

where

$$y = (\ln L \ln L_{50})/\sigma_{\ln L} \quad (4)$$

Here, L_{50} is the median diameter. If L=L_{50}, then y=0 and $\Phi_{(y=50)}$=1/2. The parameter $\sigma_{\ln L}$ characterises the width of distribution and indicates the deviation of logarithm of size from ln L_{50}.

In practice, in treating granulometric data, the function $\Phi(L)$ is first plotted and then, using integral tables, the value of the argument, y, can be determined and the dependence of y on ln L can be plotted. If the particle distribution corresponds to the log-normal distribution, then the data will describe a linear array in (y, ln L) space. Then, from the plot parameters of the function

$$y = A + B \ln L \quad (5)$$

we obtain

$$\sigma_{\ln L} = 1/B; \ln L_{50} = -A\sigma_{\ln L} \quad (6)$$

The correspondence of particle size distribution of fragments to Rosin-Rammler or log-normal distributions is interpreted to result from the differing character and mechanisms of fragmentation (Rodionov et al. 1986) in each case. Below we use the approach of Schleyer (1987) to compare the fit of our data to both distributions. As it is unusual to obtain a perfect distribution, Schleyer analysed the truncation of the distribution curves and the effect of such truncation to the log-normal and the Rosin-Rammler approach. Importantly, he found that even if a curve is significantly truncated, the torso of the distribution can be used for the calculation of the fit. The calculation can be used to recalculate the missing tails of the truncated distribution, and thereby provide important information.

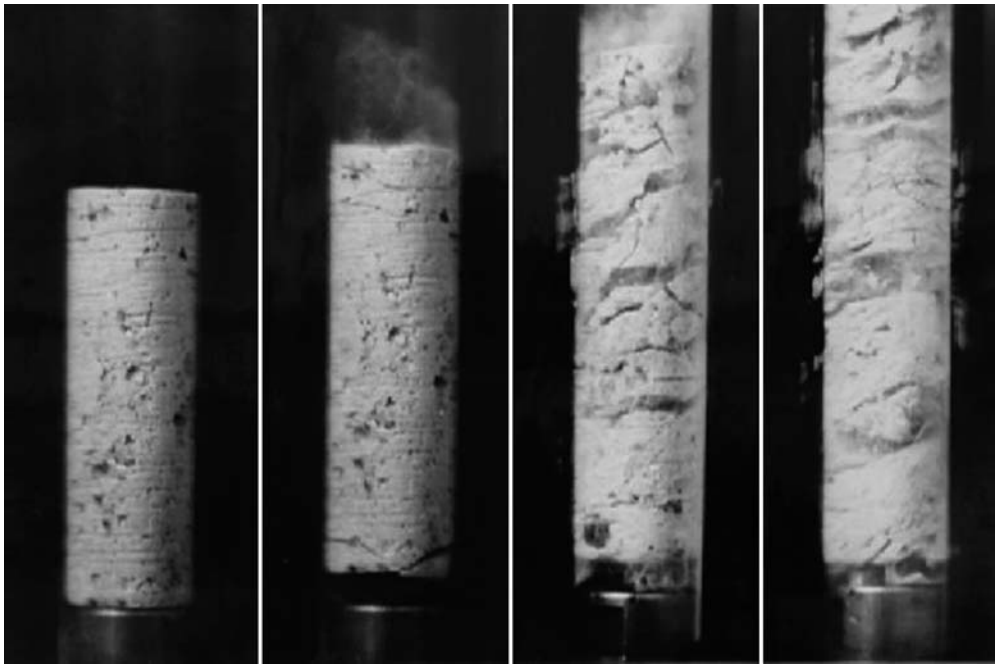

Fig. 1 A sequence of still photographs of fragmenting pumice samples (Santorini) at time intervals of 0.25 ms. A Plexiglas autoclave was used to visualise the fragmentation process on a cylindrical sample of 50-mm length and 20-mm diameter. The first frame at 0 ms shows the sample in the original state prior to the diaphragm opening. In the second frame at 0.25 ms after diaphragm rupture, fine dust ejects from the sample surface, i.e. the rarefaction wave has already reached the sample surface. The bottom of the sample is detached from the holder. A possible mechanism for the detaching is the elastic response to the unloading wave. Note that the lower edges of the sample are broken. The third frame (new sample) at 0.5 ms demonstrates the propagation of the fragmentation wave. The upper 30 mm of the sample is fragmented ± perpendicular to the axis of decompression. In the fourth frame, the complete fragmentation of a sample at 0.75 ms and the ejection of the particles are demonstrated

Results

Fragmentation threshold

The experiments demonstrate that at room temperature, fragmentation of dacite samples occurs at minimum a pressure differential between HPT and LPT of ΔP_0~9 MPa. At these pressure differentials only a few, flat, platey particles are removed from the cylinder surface. Below this value of pressure drop, no fragmentation occurs. At ΔP_0 only slightly exceeding 9 MPa, the upper end of the sample typically fractures into a small number of pieces. Raising ΔP_0 causes more effective fragmentation and ejection of fragments into the LPT. An increase of the experimental temperature causes a lower fragmentation threshold. At high temperature=900 °C, the dacite fragmentation occurs with a pressure differential of 3 MPa.

Although in these experiments the first fragmentation occurs at 3 MPa, the fragmentation threshold should be viewed as a minimum differential fragmentation pressure ΔP_{fr}. In nature, pre-stressing and anisotropic stress components may either reduce or even increase this number by several MPa.

Morphology/texture of fragments

Optical microscopy and SEM study of fragments reveal that the largest fragments exhibit plate-like shapes due to the fact that the fracture surfaces are oriented normal to the sample axis (Fig. 1). Small fragments have more equant shapes than large fragments. Large particles (approx. 1 mm) usually consist of crystals in a vesicular groundmass. In some cases the characteristic size of fragments is comparable with that of crystals. Smaller fragments (~0.1 mm) may consist solely of either crystal fragments, vesicular glass shards or crystals with remnants of vesicular glass. No evidence was found that microlites influence the shape of the fragments. The texture of fragments is illustrated in Fig. 2 where SEM images of fragments from experiments with T=18 °C are presented. The structure of such fragments is clearly visible on the SEM images and is identical for fragments of all temperature ranges (Fig. 2). The SEM analysis also reveals cracks on the surface as well as within fragments. Such cracks are observed in fragments obtained from experiments at all temperatures. Fractures in phenocrysts can not be easily distinguished as new versus relict cracks since all large crystals in the grey dacite were already fractured prior to the experiments. One of the most characteristic features of the experimental fragments of the Mount St. Helens grey dacite is their angular shape,

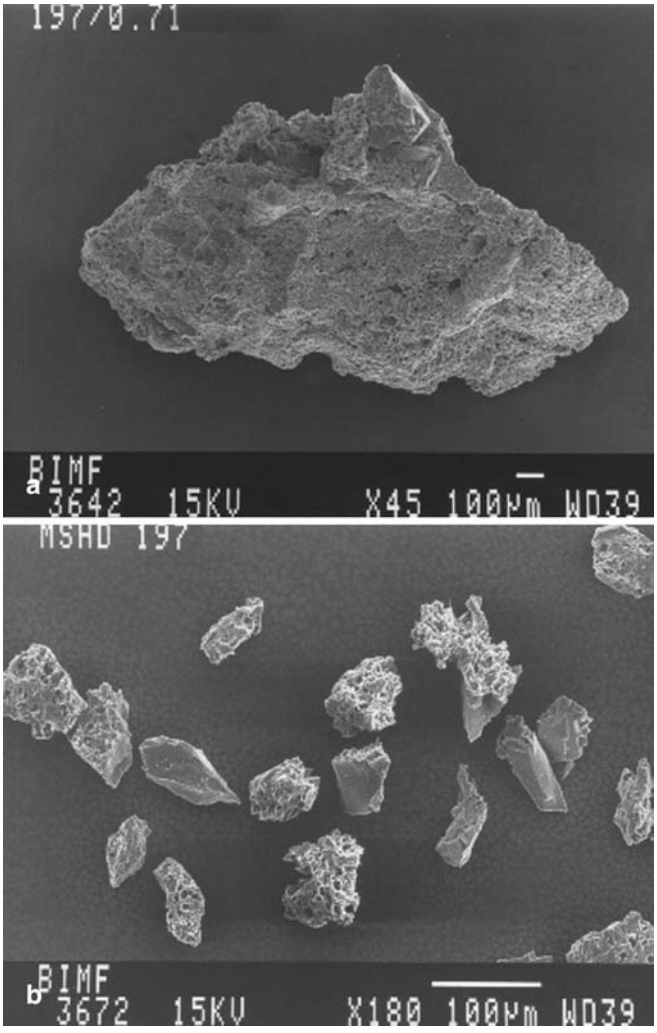

Fig. 2a, b SEM image of fragments of experiment #197, T_0=18 °C and ΔP_0=11.8 MPa. **a** >0.71-mm fragment. On the upper edge a crystal fragment is visible. **b** Crystal and matrix fragments <63 µm. The ratio of crystal to glass matrix is identical to the starting material. The grain morphologies from high-temperature experiments are indistinguishable from those of low-temperature runs

observed in sets of experiments at T~18 °C (room temperature) as well as at T=750 (i.e. T<T_g), 810 (i.e. T=T_g) and 900 °C (i.e. T>T_g). Clear evidence of viscous deformation is thus absent. It should be noted that the highest experimental temperature reported here (900 °C) exceeds the dilatometrically determined glass transition temperature (T_g~800–810 °C; 10 °C min^{-1}) of the rhyolitic melt phase in the grey dacite. SEM study and image analysis of polished sections of fragments from experiments at different temperatures do not reveal any foaming or additional vesiculation of the dacite in comparison with the vesicularity of the original material. The vesicles have the same shape and size in both the pre- and post-experimental state. Additional investigations of vesicularity of fragments from experiments performed at T=18 and 900 °C conducted using mercury porosimetry also did not reveal changes in vesicle size distributions (Fig. 3a–c). Peaks in the curves of the vesicle size distribution for starting material and experimental fragments were located at the same place with the exception of the peak corresponding to the collapse of the closed porosity (short distance connected) existing only with the starting material (Fig. 3a).

Grain-size characteristics of fragments

The fragments generated exhibit a wide distribution of grain sizes. The largest size was comparable to the diameter of the sample (17 mm). The median diameter of fragments (Md_φ) ranges from –0.4 to –3.5 φ units, the mean diameter of fragments (M_φ) from –0.15 to –2.6 φ, and the sorting coefficient (σ_φ) from 1.1 to 2.1 φ.

Effect of temperature

Experimental temperature influences the grain-size characteristics of fragments. With an increase of temperature, the grain-size distribution curves become more asymmetric and the peak on the frequency grain-size distribution curves shifts in the direction of larger fragments (Fig. 4). Additionally, for experiments performed at room temperature, and at an initial pressure differential of ~12 MPa and calculated decompression rate of $|dp/dt|$~40 MPa ms^{-1}, the frequency distribution of the grain size has a single mode whereas sets of experiments performed at T≥750 °C often exhibit bimodal distributions. The experiments performed at a maximum temperature of 900 °C demonstrate uni- and bimodal distributions. The bimodality corresponds to incomplete fragmentation of the sample (we record single large particles) and can not be correlated to material constraints like the size of phenocrysts, as in experiments on basaltic andesites from Merapi (Spieler and Dingwell 1998).

The trend of increasing fragment size with increasing temperature is also apparent in the Md_φ–σ_φ diagram (Fig. 5) where four sets of experiments generate four distinct, overlapping clusters. By contrast, variations in the sorting coefficient σ_φ are not as large, and a regression line of the experimental data in the Md_φ–σ_φ diagram reveals an essentially insignificant variation in σ_φ with increasing temperature.

Particle size distributions of fragments obtained from experiments at T=20, 750 and 900 °C and ΔP_0~12 MPa, plotted as a log-normal vs. Rosin-Rammler goodness-of-fit diagram (Schleyer 1987), are presented in Fig. 6. It can be seen that, with the exception of an incomplete, fragmented experiment (750 °C, 13.1 MPa), none of the derived distributions correspond to log-normal distributions. The fragments from the experiments conducted at low temperature (20 °C) exhibit a closer approach to the Rosin-Rammler distribution curves whereas experiments conducted at high temperature (900 °C) fall closer to the partition line against the log-normal distribution field. We assume that truncation of the data set due to (1) experimental

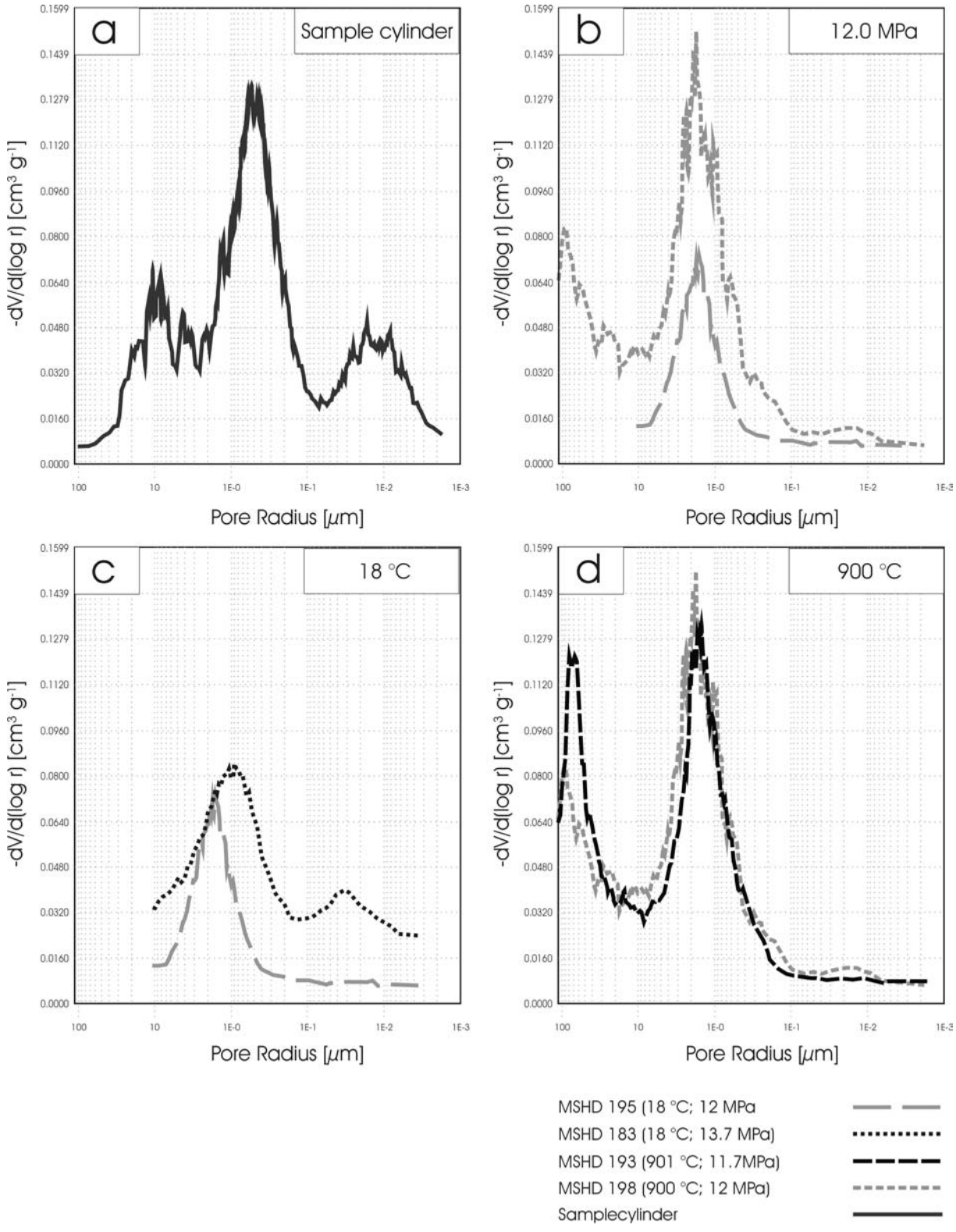

Fig. 3a–d Results of the Hg porosimetry. Pore-size distribution in the original sample and fragments derived from experiments performed at different temperatures, pore radius (μm) vs. –dV/d(log *r*) (cm^3 g^{-1}). **a** Pore-size distribution in the original sample. **b** Experiment #195, T=18 °C and ΔP_0=12.0 MPa vs. experiment #198, T=900 °C, ΔP_0=12.0 MPa. **c** Experiment #195, T=18 °C, ΔP_0=12.0 MPa vs. experiment #183, T=18 °C, ΔP_0=13.7 MPa. **d** Experiment #193, T=901 °C, ΔP_0=11.7 MPa vs. experiment #198, T=900 °C, ΔP_0=12.0 MPa. The shift of the pore radius from 0.5 to 1–1.5–2 μm is a result of cutting the connected pores by fragmentation. The same effect opens the "closed porosity" (1E–2 μm). The existence of the closed porosity peak in the analysis of experiment MSHD 183 appears to correspond to a denser starting material

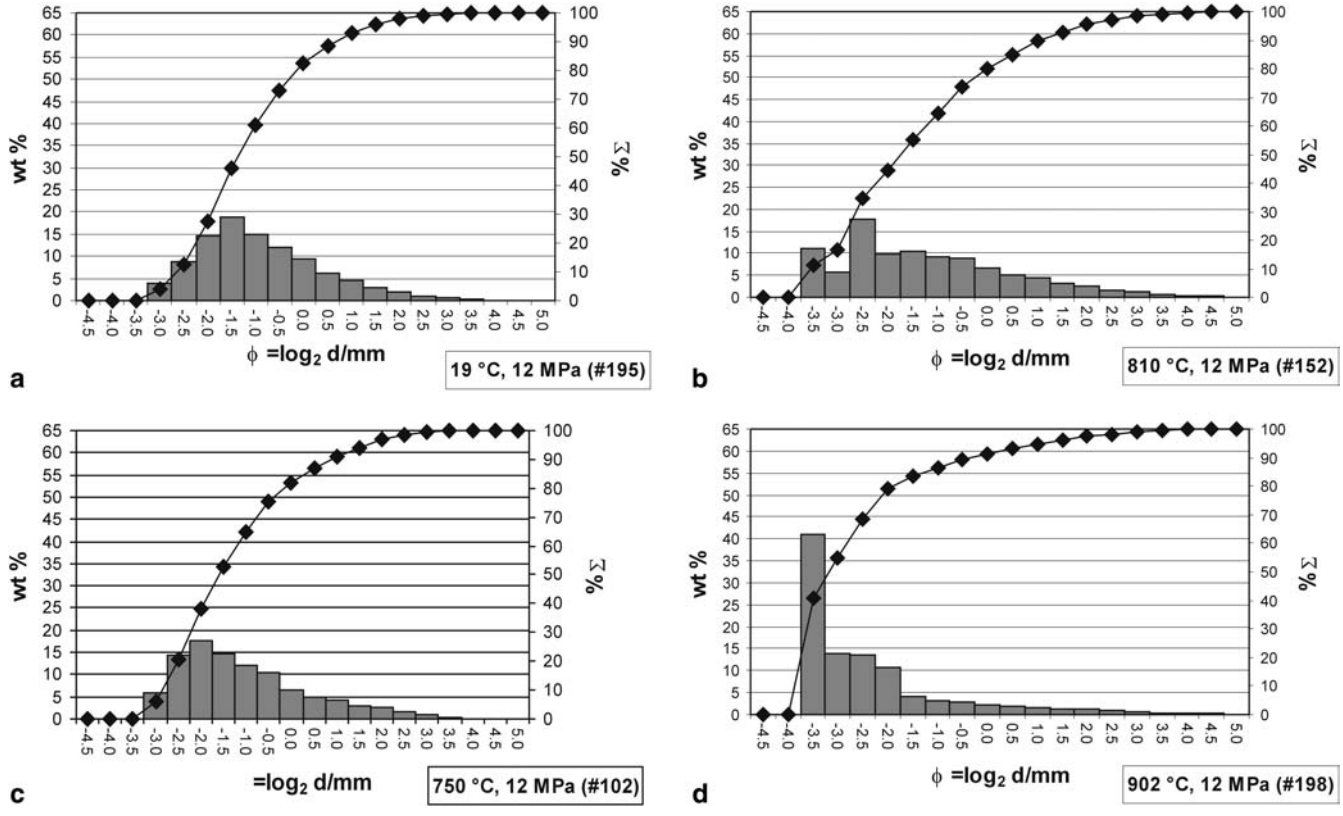

Fig. 4a–d Effect of temperature on the frequency grain-size distribution and cumulative curves from experiments performed at ΔP_0=12.0 MPa and different temperatures. Experiments #195 at T_0=19 °C (**a**), #102 at T_0=750 °C (**b**), #152 at T_0=810 °C (**c**), and #198 at T_0=902 °C (**d**) are a tentative demonstration of the dependence of fragmentation efficiency on the density of the gas phase. This can account for the faster transition to smaller grain sizes at the low-temperature experiments with increasing pressure drop compared to the high-temperature analogue experiments

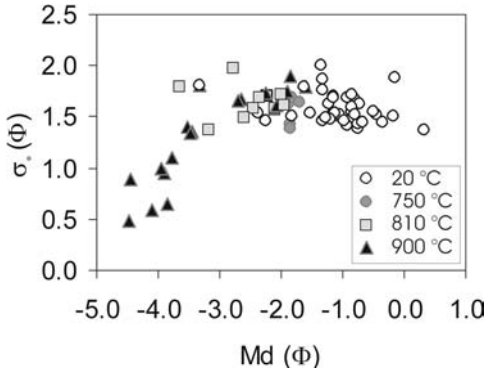

Fig. 5 Sorting coefficient vs. median diameter (Md_φ) for experiments at varying temperature. The 900 °C results are influenced by the large fragments in the experiments close to the threshold pressure. They still give a linear trend which can not be recognised with the experiments at 810, 750 and 20 °C

restriction by sample size, and (2) the loss of fine particles occurs in our experiments. However, the proof of the original Rosin-type distribution is possible for the torso of the data, since in Figs. 6 and 7 the plot of the Gauss vs. Rosin test of Schleyer clearly proves the Rosin distribution.

Effect of pressure

The effect of initial pressure differential (ΔP) on the frequency grain-size distribution curves of fragments obtained in experiments performed at T=18 °C is demonstrated in Fig. 8a–d. It can be seen that the pressure increase causes a shift of distribution peaks in the direction of smaller sizes. The weight percentage of single, large fragments in the experiments is high. This has a major influence on the mass distribution of the sample, and the statistical interpretation needs close examination of its validity. The frequency distribution curves of fragments obtained in experiments performed at T=900 °C (Fig. 8e, f) demonstrate the same problem.

The dependence of median diameter of fragments on initial pressure differential (ΔP) is presented in Fig. 9a, b for two sets of experiments conducted at temperatures T=20 and 900 °C. The effect of initial pressure differential on the 36.79 percentile of fragments seems most significant in the range of low initial pressure differential. It is an effect of incomplete sample fragmentation close to the threshold. Since the grain-size distribution curves of the dacite correspond more to the Rosin-Rammler distribution than to the log-normal distribution, we plot the percentile of 36.79 which corresponds to the median

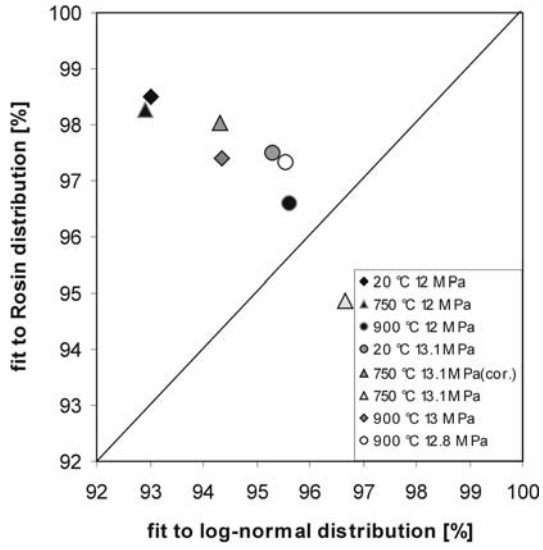

Fig. 6 Log-normal vs. Rosin diagram of experiments with rising temperature at two initial differential pressures. *Closed symbols* correspond to experiments at 12.0 MPa, and *shaded symbols* to 13.0-MPa initial pressure difference. The experiment at 750 °C and 13.1 MPa had to be corrected since a large piece of the sample did not fragment and thus ruled out statistical analysis (*open triangle* uncorrected data). By removing the weight of the single particle, the data fell back on the Rosin curve. The close match of data by repeated experiments is demonstrated by experiments at 900 °C/ 13.0 MPa and 12.8 MPa respectively

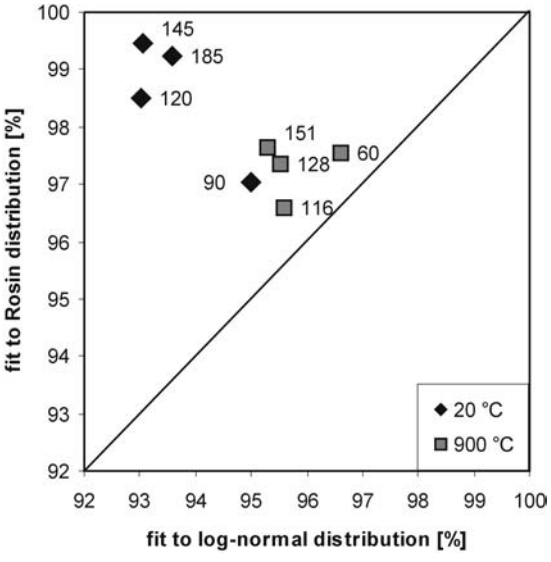

Fig. 7 The question as to whether a log-normal or Rosin distribution is produced due the first decompression-controlled fragmentation of magma in a conduit can be analysed using the Gauss vs. Rosin diagram (calculation after Schleyer 1987). The *labels* give ΔP in MPa. The better fit of the low-temperature data is due the higher degree of fragmentation. The data points correspond to the experiments presented as size distribution curves in Fig. 3a–d

(50%) of the log-normal distribution. The dependence of the 36.79 percentile on initial pressure differential is stronger for the set of high-temperature experiments (T=900 °C) than for the experiments at low temperature (T=20 °C).

It should be noted that truncation of distribution curves at the coarse or fine end influences the precision of the statistical tests. Schleyer (1987) presented the correlation of log-normal vs. Rosin distribution as grain-size parameter and investigates the effects of truncation. Again, note that the experimental sets are truncated at both ends: (1) truncation at the coarse end of the distribution is method-based (size of sample cylinders); (2) the loss of fine particles in sampling leads to a truncation of the fine end. Thus, recalculation has to focus on the torso of the curves.

Discussion

On a μs time scale the effective viscosity at the glass transition is a million times less than that dilatometrically determined, on the order of 10^6 Pa s (Dingwell et al. 1993; Dingwell 1995, 1996). Samples more viscous than this value are not expected to exhibit viscous deformation during fragmentation.

We found in experiments on less viscous hydrous HPG8 silicate melts that post-fragmentation foaming tends to smooth the edges of the particles. If the particle is cooled slowly enough, rehealing of surfaces is possible (Martel et al. 2000).

Plate-like shape of large fragments and fragmentation mechanics

The plate-like shape of large fragments demonstrates that dacite sample fracturing occurs through planes normal to the direction of the decompression (i.e. the long axis of the sample; Fig. 1). This direction coincides with the direction of the application of tensile stresses during the rapid decompression. The observed (short-time still photography of cold experiments using a Plexiglas autoclave and by particles which can be reoriented to form stacks, like a stack of plates) plate-like shape of the fragments can be explained within the framework of the recently described mechanism of porous material fragmentation by rapid decompression (Alidibirov 1994; Alidibirov and Dingwell 2000). Experimental studies on the dynamics of fragmentation of porous materials containing excess gas pressure undergoing rapid decompression demonstrated that the "fragmentation wave" mechanism plays a major role. The direct observation of the fragmentation of porous material using high-speed cameras (Alidibirov and Panov 1998) has demonstrated that the first parallel fractures separating the sample became visible in the upper part of the sample, where decompression first occurs. The particles are accelerated and ejected into the LPT while a new plane of fractures forms parallel or sub-parallel to the new surface. The

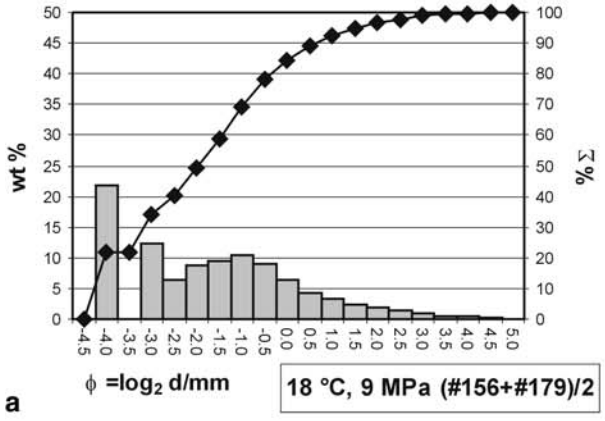
wt %
Σ %
ϕ =log2 d/mm
18 °C, 9 MPa (#156+#179)/2

a

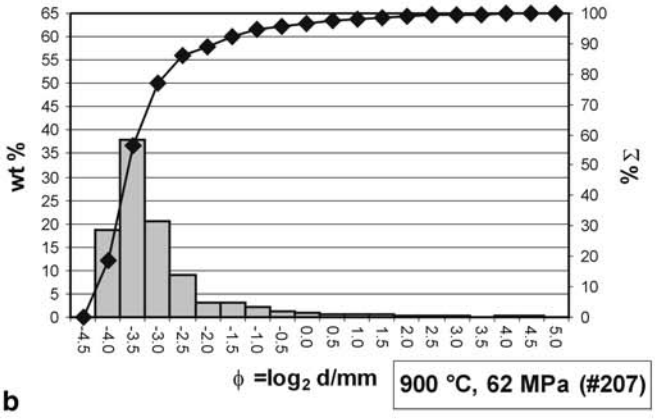
wt %
Σ %
ϕ =log2 d/mm
900 °C, 62 MPa (#207)

b

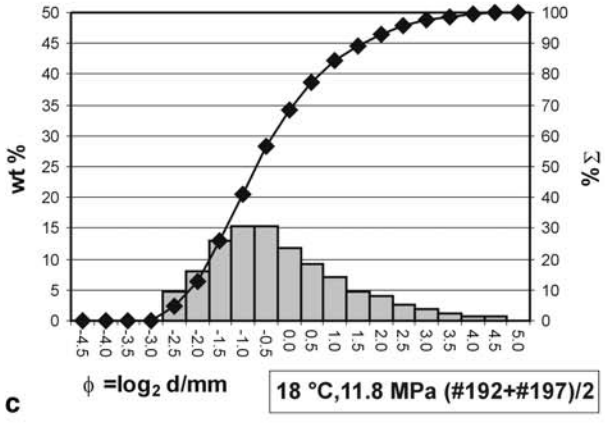
wt %
Σ %
ϕ =log2 d/mm
18 °C,11.8 MPa (#192+#197)/2

c

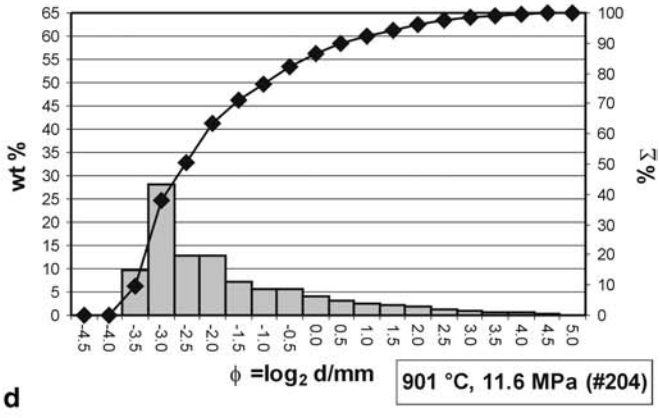
wt %
Σ %
ϕ =log2 d/mm
901 °C, 11.6 MPa (#204)

d

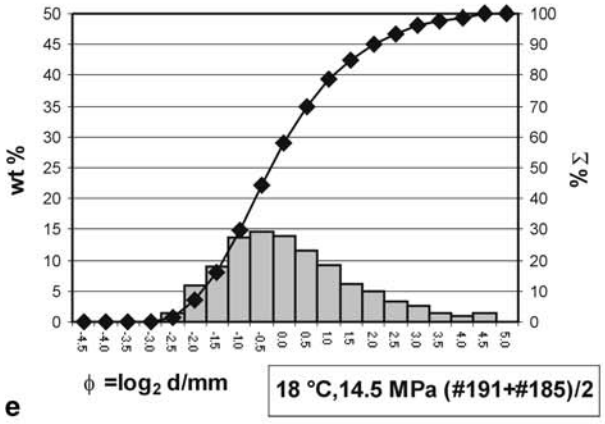
wt %
Σ %
ϕ =log2 d/mm
18 °C,14.5 MPa (#191+#185)/2

e

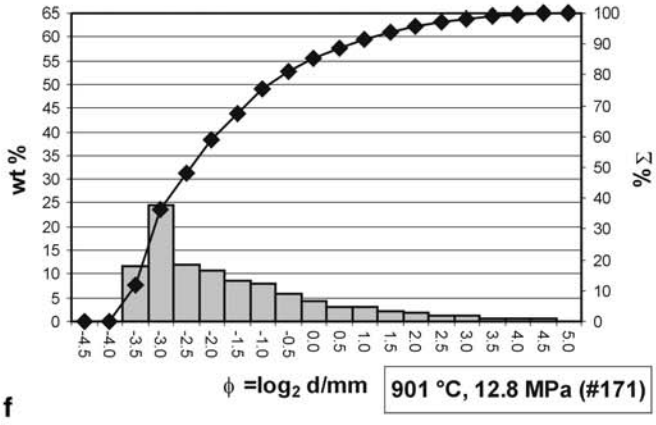
wt %
Σ %
ϕ =log2 d/mm
901 °C, 12.8 MPa (#171)

f

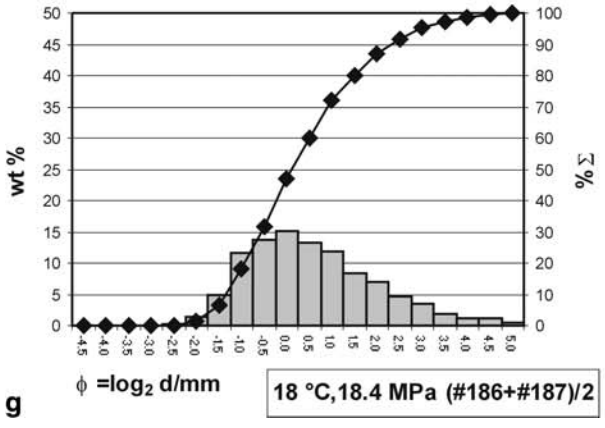
wt %
Σ %
ϕ =log2 d/mm
18 °C,18.4 MPa (#186+#187)/2

g

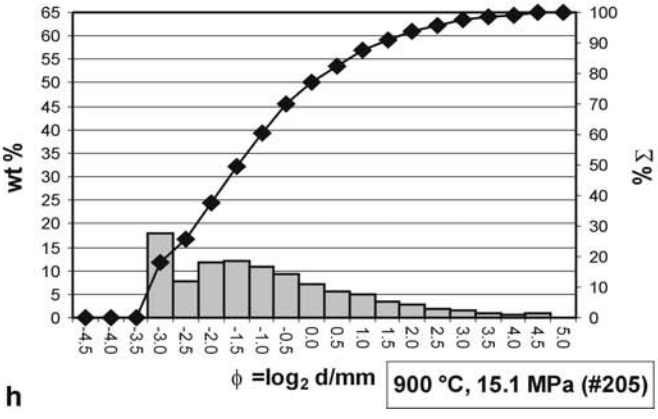
wt %
Σ %
ϕ =log2 d/mm
900 °C, 15.1 MPa (#205)

h

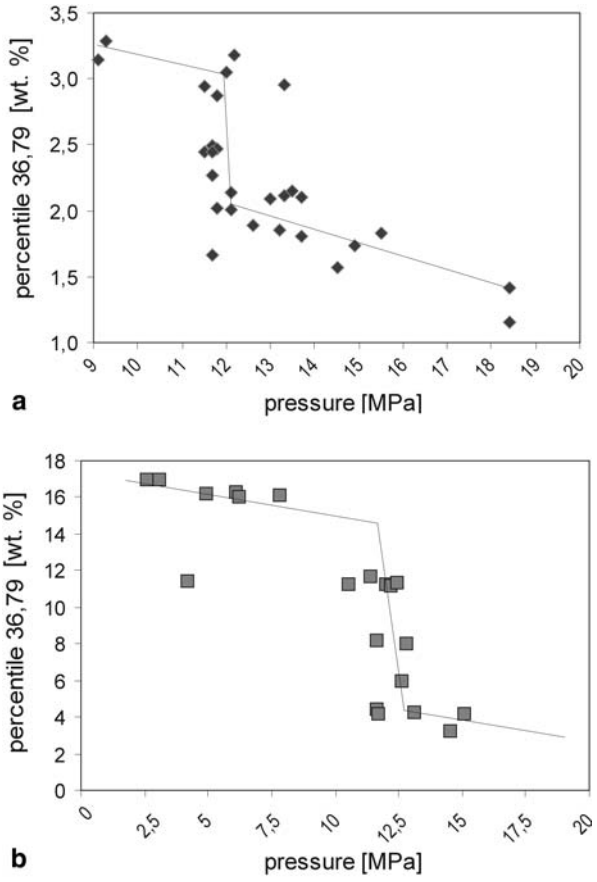

Fig. 9a, b The plot 36.79 percentile vs. ΔP pressure (MPa) demonstrates the fragmentation behaviour of MSHD at ~20 °C (**a**), and at 900 °C (**b**). The distribution seems to prove the theory that the fragmentation occurs according to the texture of the rock specimen. For a start, the megascopic texture controls the fracture growth and then, at 11 MPa (~20 °C) and 10 MPa (900 °C) respectively, the macroscopic texture (vesicles and crystals) rules the fragmentation process. At ~12.5 MPa (20 °C) and 15 MPa (900 °C), the microscopic (density-controlled) texture influences the particle size. Since the grain-size distribution curves of the dacite correspond better to the Rosin distribution rather than following the ideal log-normal distribution, we plot the percentile of 36.79 [which corresponds to the median (50%) of the log-normal system]. The differentiation of the three texture-controlled regimes is better pronounced in the 20 °C experiments. Note that the density difference of the gas phase is high. At 20 °C and 12.0 MPa the density of the gas phase is 19.8×10^{-5} kg m^{-3} and reduces to 4.9×10^{-5} kg m^{-3} at 900 °C

Fig. 8a–h Frequency grain-size distribution curves and cumulative grain-size distribution curves of experiments at 18 and ~900 °C at changing pressure. It can be seen that the pressure increase causes a shift of distribution peaks in the direction of smaller sizes. The weight percentage of single, large fragments (>–3Φ) in the experiments is high. Thus, single particles may have a major influence on the validity of the statistical interpretation. The distribution curves of fragments obtained in experiments performed at T=18 °C (**a–d**) and at T=900 °C (**e–h**) demonstrate the similar behaviour. Close to the fragmentation threshold at 900 °C (ΔP_{fr}=3 MPa), the low ΔP of 4.2 MPa produces the highest mass fraction of large fragments

process of a sequential appearance of fractures propagates until the pressure difference falls below the ΔP_{fr}. This process explains the appearance of the platy particles in the experiments and in some natural deposits of explosive eruptions. The propagation of the fragmentation wave front through the sample can be used to calculate the speed of the magma fragmentation (Spieler et al., unpublished data). We take the angular shape of the fragmentation products as indicative of brittle fragmentation of the magma samples. Since the angularity of the fragments is observed over the entire experimental temperature range (18–915 °C), we deduce that the duration of the rapid decompression forces the highly viscous vesicular dacite to behave like a solid. The preservation of the brittle fragmentation features on the particles is possible if the viscosity of the fragmented melt is high or if the cooling time is shorter than the ductile healing of the surface features.

The brittle-like behaviour can be explained by taking the experimental conditions and the dacite properties into account. The stress on the bubble walls caused by the rapid decompression of a dacite sample can overcome the tensile strength of the glass crystal mixture.

In nature, nonhydrostatic stress components may either reduce or even increase the experimentally determined threshold by several percent. The important information is that, at ΔP_{fr}, the pressure is insufficient to establish a stable fragmentation front. If the porosity is small and the transportation energy of the expanding gas is too small for an extensive "pushout" of fragments, the addition of 1 MPa is sufficient to produce a stable fragmentation front. The relative thickness of the fragmentation front depends on the distribution, size and, we suspect, the interconnectivity (permeability) of vesicles in the magma.

Log-normal versus Rosin-Rammler (Weibull) behaviour of the experimental pyroclasts

Empirical distributions like a log-normal or Rosin-Rammler curve will occur only in single-phase materials. Two- or polyphase materials, like the rock samples used in the experiments presented, will follow the same law but on a more complex basis.

On a "megascopic" scale the material is statistically uniform and will follow the empirical Rosin-Rammler law of crushing, or exhibiting a log-normal distribution. Where the fragmentation regime passes into the macroscopic scale, we are confronted with a multicomponent material. The fragmentation mechanism is then influenced by variable phase density, viscosity and elasticity, leading to multicomponent curves accompanied by nontrivial stress distributions and concentrations. For these reasons, Martel et al. (2000, 2001) have attempted to systematise the textural control on fragmentation efficiency.

In the range of our experiments, the dacite of Mt. St. Helens reacts with only minor deviations from the behaviour expected of a uniform material. Nevertheless,

the influence of the material constraints can be demonstrated in terms of grain-size parameters versus initial pressure difference (Fig. 9).

Effects of temperature and initial pressure differential on fragment size

Among the factors governing the characteristic fragment size observed in our experiments are temperature, initial pressure differential, and the internal structure of the sample. The effect of temperature demonstrated in Figs. 4, 5, 6, 7, 8 and 9 proves that the lower the temperature, the higher the efficiency of the fragmentation at a given ΔP. In a plot of the 36.79 percentile vs. ΔP (Fig. 9a, b), we demonstrate that the influence of low temperature nearly erases the structural influence. We propose that this effect occurs, since at low temperatures the reduced elastic response equals the brittle state of all condensed phases in the samples.

In general, we see that the higher the ΔP_0, the steeper is the pressure gradient near the free surface of the fragmentation front and the thinner the layer of the dacite which will be broken away (Alidibirov and Panov 1998). For the finest or density-controlled sector of the distribution presented, the "fragmentation wave" mechanism will be overridden when crystals of a narrow size distribution are present or a uniform foam is fragmented (Fig. 11a, b).

Effects of material structure on fragment size

The effect of material structure is best recognised in a plot of Md_{φ} vs. ΔP_0. Since the grain-size distribution curves of the dacite correspond to the Rosin distribution rather than follow the log-normal distribution, we plot the percentile of 36.79 which corresponds to the median (50%) of the log-normal system. The 36.79 percentile of fragments d obtained in the experiments demonstrates a complex dependence on the initial pressure differential ΔP_0 (Fig. 9a, b) with the material structure on different scales. In both plots the distribution appears to support the notion that the fragmentation depends on the texture of the rock specimen. Firstly, the megascopic texture (scale of metres to centimetres) dominates the efficiency of low-pressure fragmentation (left domain Fig. 9a, b). Secondly, the macroscopic (centimetre to 100 μm) texture controls the fragmentation (vesicles, crystal size and integrity) and, at ~12.5 MPa, the microscopic texture (100 μm to submicron) the mechanical properties of the condensed phases themselves, influence the particle size. Finally, when the energy transmitted into the system generates particles smaller than the pre-existing crystals and microlites, the fragmentation process will become complex. The crystals will only react elastically. If crystals have melt inclusions, the pressure inside the inclusion will decrease the fracture toughness of the crystals. Therefore, it will be possible that a decompression wave due to unloading will fragment the crystal prior to the fragmentation wave mechanism. If inclusions already opened due to fragmentation of the crystals, then the fragments contain no significant energy. This phenomenon corresponds to a density-controlled fragmentation, where the denser sites of the material need much higher energy input into the system to fragment.

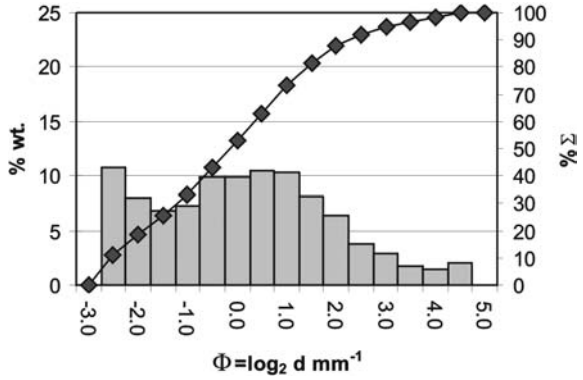

Fig. 10 Particle distribution curve of experiments on Merapi andesite at 18 °C and 13.1 MPa. The curve describes a distribution with a modification due to plagioclase phenocrysts relatively more dense than the bulk magma. A second phenomenon, the "safety net structure" (Spieler and Dingwell 1998), enhances crystal survival

Two results which are not developed in Mt. St. Helens dacite (due to its pre-fragmented crystals and the size distribution of the vesicles) should nevertheless be mentioned in the context of material structure. The first case is given with the presence of crystals of a narrow size range. In Merapi andesite the presence of plagioclase (~800 μm) was identified in the granulometric analysis of experimental and natural pyroclasts. The distribution curve presented in Fig. 10 shows a bimodal distribution with a peak around 0.5ϕ. The bimodality accounts for the crystals and crystal fragments which contain no vesicles or melt inclusions and react during decompression only to their elastically stored energy. The second case presented is an analogue material, an insulation foam (Coriglas). Coriglas is a glass foam with near-unimodally distributed vesicles. Experiments to understand the secondary fragmentation in the fragmentation bomb (unpublished data) have revealed that during decompressive fragmentation, a foam reacts according to its density distribution (Fig. 11a). The vesicle joints build a microstructure which has a higher density with respect to the bulk material. Few or no vesicles are found at the junction point, and thus only elastically stored energy is released at these sites. The curve in Fig. 11a shows a peak corresponding to the size of the joint diameter. The fact that much higher energy is necessary to fragment the denser sites is shown in Fig. 11b, where a steel plate was placed 40 cm above the autoclave in the trajectory of the ejected particles. Only a minor shift of the second peak is revealed but the majority of the large particles has been destroyed and accumulated as fines. Here we see that the experimental approach of Kaminski and Jaupart (1998) apparently fails for the decompression case. In experiments on Merapi

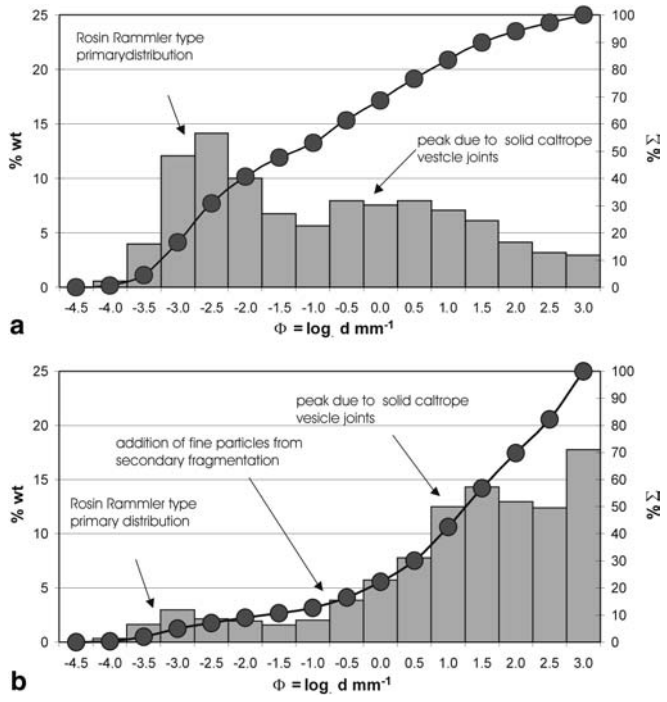

Fig. 11 **a** Particle distribution curve of single fragmentation, "no plate" experiments on Coriglas at 21 °C and 4 MPa. The curve describes a perfect Weibull distribution for the large particle sizes to 0.75 mm. The modification of the curve is due to caltrope and triaxial vesicle joints relatively more rigid than the total material. **b** Particle distribution curve of secondary fragmentation "steel plate" experiments at 21 °C and 4 MPa. The majority of the large particles (>0.5 mm) is fragmented by a secondary fragmentation process on the plate suspended for that purpose in the fragment trajectory. By the addition of "secondary" fine particles, we get a typical, fine-end-dominated distribution curve. Caltrope and triaxial vesicle joints represent dense structures which are more rigid than simple vesicle walls. The dense structure survives even the secondary fragmentation and modifies the extreme deformed curve

andesite (Spieler and Dingwell 1998) and on synthetic rhyolitic systems (Martel et al. 2000, 2001), we have clearly observed that crystals can have an influence on grain size. Why do we see no effect for the fragmentation of the grey dacite of Mt. St. Helens? This is due to the relative size of the shattered crystals fragments with a M*d* of 270 μm and a Gaussian distribution. The influence is thus simply not distinguishable in the present data.

Compared to the size of the experimental pyroclasts, the modifying effect of the crystals on the distribution curve is extremely small. Secondary fragmentation and abrasion should however increase the sensitivity of the grain-size distribution to the crystal sizes if, as we expect, the crystals are stiffer than the matrix glass.

Comparisons to natural pyroclasts

The parameters Md_ϕ and M_ϕ of the experimental pyroclasts are close to those of the 18 May 1980 Mount St. Helens blast deposits, but the sorting coefficient (σ_ϕ) of the experimental fragments is lower than that of the natural material (Hoblitt et al. 1981). Despite the close correspondence of the median diameters of the data, we caution that this comparison is very fragile. In nature, pyroclasts experience a number of transport and by this, sorting phenomena which may exert their influence on the grain-size distribution (Wohletz et al. 1989). For the experimental pyroclasts, which demonstrate the Rosin-Rammler distribution, we find the experimental restrictions on the grain size exhibited especially in the sorting coefficient. The maximum size of the experimental fragments was given by the diameter of the sample cylinders (17 mm), where for the natural case such restrictions are not given. Nevertheless, a close similarity between experimental and natural fragments of the grey cryptodome dacite lies in the angular shape of the pyroclasts, reflecting the brittle fragmentation during decompression. The experimental conditions of the high-temperature experiments (900 °C and initial pressure difference ΔP_0~3–20 MPa) were close to those estimated for the 1980 cryptodome (Eichelberger and Hayes 1982). Thus, the similarity in shape can be used to conclude that brittle fragmentation was the essential mechanism during the 1980 lateral blast of the Mount St. Helens cryptodome.

Summary

1. Experiments on the fragmentation of the 1980 Mount St. Helens grey cryptodome dacite performed at T=18–900 °C and initial pressure differentials up to 18.5 MPa demonstrate the effect of temperature on dacite fragmentation: (1) the fragmentation threshold decreases from 9 to 3 MPa with temperature increase from 18 to 900 °C, and (2) a coarsening of the 36.79 percentile with the increase in temperature is observed. Both effects can be explained by the decrease of the threshold strength at higher temperatures which also influences the characteristic size of fragments. It is possible that the lower density of the gas phase has some influence on the energy conversion forming the particles. Experiments demonstrate also the effect of pressure drop: a decrease in the median diameter with the increase in the initial pressure differential is observed.
2. Angular shape of fragments is observed at all temperatures, even at 900 °C (well above the dilatometrically determined glass transition temperature of 810 °C). Note that due to the short time scale of the rapid decompression, we force the melt over the glass transition into the brittle field, and thus brittle-like behaviour must occur under rapid decompression (Dingwell 1996).
3. Fragment size distributions of the rapid decompression experiments are clearly described by the Rosin-Rammler law.
4. Comparison of characteristics of experimental and natural fragments of the grey cryptodome dacite of the

Mt. St. Helens 1980 eruption shows similarity in the shape of fragments and demonstrates similar median diameters.

Acknowledgements This work was supported by the Alexander von Humboldt Foundation, the European Commission, the Deutsche Forschungsgemeinschaft (Di-431) and the Bayerisches Geoinstitut. We are grateful to R. Hoblitt and C.D. Miller for providing samples of Mount St. Helens dacite and encouragement, as well as to H. Grönig, M. Lennarts, P. Neuwald and H. Keppler for useful experimental advice, G. Herrmannsdörfer for technical assistance, K. Klasinski and R. Weigel for development of computer codes and electronic equipment, H. Schulze for sample preparation, C. Drummer for assistance with SEM study and R. Schleyer for kindly placing his Fortran program at our disposal. The reviewers J. Taddeucci and K. Wohletz helped to improve the paper.

References

Alidibirov M (1994) A model for viscous magma fragmentation during volcanic blasts. Bull Volcanol 56:459–465

Alidibirov M, Dingwell DB (1996a) Magma fragmentation by rapid decompression. Nature 380:146–148

Alidibirov M, Dingwell DB (1996b) An experimental facility for the investigation of magma fragmentation by rapid decompression. Bull Volcanol 58:411–416

Alidibirov M, Dingwell DB, Stevenson RJ, Hess K-U, Webb SL, Zinke J (1997) Physical properties of the 1980 Mount St. Helens cryptodome magma. Bull Volcanol 59:103–111

Alidibirov M, Panov V (1998) Magma fragmentation dynamics: experiments with analogue porous low-strength material. Bull Volcanol 59:481–489

Alidibirov M, Dingwell DB (2000) Three fragmentation mechanisms for highly viscous magma under rapid decompression. J Volcanol Geotherm Res 100:413–421

Barclay J, Riley DS, Sparks RSJ (1995) Analytical models for bubble growth during rapid decompression of high viscosity magmas. Bull Volcanol 57:422–431

Bennett FD (1974) On volcanic ash formation. Am J Sci 274:648–661

Brown WK, Wohletz KH (1995) Derivation of the Weibull distribution based on physical principles and its connection to the Rosin-Rammler and lognormal distributions. J Appl Phys 78(4):2758–2763

Cashman KV (1988) Crystallization of Mount St. Helens 1980–1986 dacite: a quantitative textural approach. Bull Volcanol 50:194–204

Cashman KV, Mangan MT (1994) Physical aspects of magmatic degassing II: Constraints on vesiculation processes from textural studies of eruptive products. Rev Mineral 30:447–478

Dellino P, LaVolpe L (1995) A model to reconstruct the behaviour of grain size distribution in Plinian fallout deposits. Periodico di Mineralogia 64:157–159

Dingwell DB, Webb SL (1989) Structural relaxation in silicate melts and non-Newtonian melt rheology in geological processes. Phys Chm Mineral 16:508–516

Dingwell DB, Webb SL (1990) Relaxation in silicate melts. Eur J Mineral 2:427–449

Dingwell DB (1995) Relaxation in silicate melts: some applications. Rev Mineral 32:21–66

Dingwell DB (1996) Volcanic dilemma: flow or blow? Science 273:1054–1055

Dingwell DB, Bagdassarov NS, Bussod GY, Webb SL (1993) Magma rheology. In: Luth RW (ed) Experiments at high pressure and application to the Earth's mantel. Mineral Assoc Can Short Course Handb 21:131–196

Eichelberger JC, Hayes DB (1982) Magmatic model for the Mount St. Helens Blast of May 18, 1980. J Geophys Res 87:7727–7738

Fink J, Kieffer SW (1993) Estimates of pyroclastic flow velocities resulting from explosive decompression of lava domes. Nature 363:612–615

Fisher RV, Schmincke H-U (1984) Pyroclastic rocks. Springer, Berlin Heidelberg New York

Hartmann WK (1969) Terrestrial, lunar and interplanetary rock fragmentation. Icarus 10:201–213

Heiken G, Wohletz K (1991) Fragmentation processes in explosive volcanic eruptions. In: Fisher RV, Smith G (eds) Sedimentation in volcanic settings. Soc Sediment Geol Spec Publ 45:19–26

Hill LG, Sturtevant B (1990) In: Meier GEA, Thompson PA (eds) Adiabatic waves in liquid-vapour systems. Springer, Berlin Heidelberg New York

Hoblitt RP, Miller CD, Vallance JW (1981) Origin and stratigraphy of the deposites produced by the May 18 direct blast. US Geol Surv Prof Pap 1250:401–420

Hoblitt RP, Harmon RS (1993) Bimodal density distribution of cryptodome dacite from the 1980 eruption of Mount St. Helens, Washington. Bull Volcanol 55:421–437

Hurwitz S, Navon O (1994) Bubble nucleation in rhyolitic melts: experiments at high pressure, temperature, and water content. Earth Planet Sci Lett 122:267–280

Ichihara M, Rittel D, Takayama K, Sturtevant B (2001) Experimental study on magma fragmentation by rapid decompression. Eos Trans AGU, 82 (47)

Kaminski E, Jaupart C (1998) The size distribution of pyroclasts and the fragmentation sequence in explosive volcanic eruptions. J Geophys Res 103:29,759–29,779

Kittleman LR (1964) Application of Rosin's distribution in size-frequency analysis of clastic rocks. J Sediment Petrol 34:483–502

Koyaguchi T (1994) Grain-size variation of tephra derived from volcanic umbrella clouds. Bull Volcanol 56:1–9

Mader HM, Zhang Y, Phillips JC, Sparks RSJ, Sturtevant B, Stolper E (1994) Experimental simulation of explosive degassing of magma. Nature 372:85–88

Mader HM, Phillips JC, Sparks RSJ, Sturtevant B (1996) Dynamics of explosive degassing of magma: observations of fragmenting two-phase flows. J Geophys Res 101:5547–5560

Martel C, Dingwell DB, Spieler O, Pichavant M, Holtz F (2000) Fragmentation of foamed silicic melts: an experimental study. Earth Planet Sci Lett 178:47–58

Martel C, Dingwell DB, Spieler O, Pichavant M, Wilke M (2001) Experimental fragmentation of crystal- and vesicle-bearing silicic melts. Bull Volcanol 63:345–359

McBirney AR, Murase T (1970) Factors governing the formation of pyroclaststic rocks. Bull Volcanol 34:372–384

Melnik O, Sparks RSJ (1999) Nonlinear dynamics of lava dome extrusion. Nature 402:37–41

Melnik O (2000) Dynamics of two-phase conduit flow of high-viscosity gas-saturated magma: large variations of sustained explosive eruption intensity. Bull Volcanol 62:153–170

Neri A, Papale P, Macedonio G (1998) The role of magma composition and water content in explosive eruptions. 2. Pyroclastic dispersion dynamics. J Geophys Res 87:95–115

Papale P (1998) Volcanic conduit dynamics. In: Freund A, Rosi M (eds) From magma to tephra, modelling physical processes of explosive volcanic eruptions. Developments in Volcanology 4. Elsevier, Amsterdam

Papale P (1999) Strain-induced magma fragmentation in explosive eruptions. Nature 397:425–428

Papale P, Neri A, Macedonio G (1998) The role of magma composition and water content in explosive eruptions. 1. Conduit ascent dynamics. J Volcanol Geotherm Res 87:75–93

Phillips JC, Lane SJ, Lejeune A-M, Hilton M (1995) Gum-rosin-acetone system as an analogue to the degassing behaviour of hydrated magmas. Bull Volcanol 57:263–268

Proussevitch AA, Sahagian DL, Anderson AT (1993) Dynamics of diffusive bubble growth in magmas: isothermal case. J Geophys Res 98:4269–4286

Rodionov VN, Sizov IA, Tsvetkov VM (1986) Fundamentals of geomechanics (in Russian). Nedra, Moscow

Rose WI, Pearson T, Bonis S (1977) Nuee ardente eruption from the foot of a dacite lava flow, Santiaguito Volcano, Guatemala. Bull Volcanol 40:53–70

Sato H, Fujii T, Nakada S (1992) Crumbling of dacite dome lava and generation of pyroclastic flows at Unzen volcano. Nature 360:664–666

Sahagian DL (1999) Magma fragmentation in eruptions. Nature 402:589–591

Schleyer R (1987) The goodness-of-fit to ideal Gauss and Rosin distributions: a new grain-size parameter. J Sediment Petrol 57:871–880

Sparks RSJ (1978) The dynamics of bubble formation and growth in magmas: a review and analysis. J Volcanol Geotherm Res 3:1–37

Sparks RSJ (1997) Causes and consequences of pressurisation in lava dome eruptions. Earth Planet Sci Lett 150:177–189

Sparks RSJ, Barclay J, Jaupart C, Mader HM, Phillips JC (1994) Physical aspects of magma degassing. I. Experiments and theoretical constraints on vesiculation. Rev Mineral 30:413–445

Spieler O (2001) Die Fragmentierung hochviskoser Magmen. Experimenteller Aufbau und Analysetechniken (in German). Electronical dissertation LMU München UMC.C 218

Spieler O, Dingwell DB (1998) Experimental fragmentation of Merapi andesite. Dtsch Geophys Ges Mitt Sonderb III:25–30

Sugioka I, Bursik M (1995) Explosive fragmentation of erupting magma. Nature 373:689–692

Thomas N, Jaupart C, Vergniolle S (1994) On the vesicularity of pumice. J Geophys Res 99:15,633–15,644

Turcotte DL (1986) Fractals and fragmentation. J Geophys Res 91:1921–1926

Voight B (1981) Time scale for the first moments of the May 18 eruption. US Geol Surv Prof Pap 1250:69–86

Voight B, Elsworth D (2000) Instability and collapse of hazardous gas-pressurized lava domes. Geophys Res Lett 27:1–4

Webb SL, Dingwell DB (1990) Non-Newtonian Reology of igneous melts at high stresses and strain rates: experimental results for rhyolithe, andesite, basalt and nephelinite. J Geophys Res 95:15,695–15,701

Wohletz KH, Brown W (1995) Particulate size distributions and sequential fragmentation / transport theory. In: Intense Multiphase Interactions. TG Theofanous and M Akiyama (eds) Proceedings of US (NSF) Japan (JSPS) Joint Seminar, Santa Barbara, CA, June 8–13, 1995, 235–241

Wohletz KH, McGetchin TR, Sanford MT III, Joner EM (1984) Hydromagmatic aspects of caldera-forming eruptions: numerical models. J Geophys Res 89:8269–8286

Wohletz KH, McQueen RG, Morrissey M (1995) Analysis of fuel-coolant interaction experimental analogs of hydrovolcanism. In: Theofanous TG, Akiyama M (eds) Intense multiphase interactions. Proc US (NSF) Japan (JSPS) Joint Sem, Santa Barbara, CA, 8–13 June 1995, pp 287–317

Wohletz KH, Sheridan MF, Brown WK (1989) Particle size distributions and the sequential fragmentation/transport theory applied to volcanic ash. J Geophy Res 94:15,703–15721

Zhang Y, Sturtevant B, Stolper EM (1997) Dynamics of gas driven eruptions: experimental simulations using CO_2–H_2O–polymer systems. J Geophys Res 102:3077–3096

Zhang Y (1999) A criterion for the fragmentation of bubbly magma based on brittle failure theory. Nature 402:648–650

Zimanowski B, Lorenz V, Fröhlich G (1986) Experiments on phreatomagmatic explosions with silicate and carbonatitic melts. J Volcanol Geotherm Res 30:149–153

Zimanowski B, Fröhlich G, Lorenz V (1991) Quantitative experiments on phreatomagmatic explosions. J Volcanol Geotherm Res 48:341–358

Zimanowski B, Fröhlich G, Lorenz V (1995) Experiments on vapour explosions by interaction of water with silicate melts. Nuclear Energy Design 155:335–343

Zimanowski B, Büttner R, Lorenz V, Häfele H-G (1997a) Fragmentation of basaltic melt in the course of explosive volcanism. J Geophys Res 102:803–814

Zimanowski B, Büttner R, Lorenz V (1997b) Premixing of magma and water in MFCI experiments. Bull Volcanol 58:491–495